

Article

Three-Saddle-Foci Chaotic Behavior of a Modified Jerk Circuit with Chua's Diode

Patrawut Chansangiam 

Department of Mathematics, Faculty of Science, King Mongkut's Institute of Technology Ladkrabang, Bangkok 10520, Thailand; patrawut.ch@kmitl.ac.th; Tel.: +66-9352-666-00

Received: 25 September 2020; Accepted: 28 October 2020; Published: 30 October 2020



Abstract: This paper investigates the chaotic behavior of a modified jerk circuit with Chua's diode. The Chua's diode considered here is a nonlinear resistor having a symmetric piecewise linear voltage-current characteristic. To describe the system, we apply fundamental laws in electrical circuit theory to formulate a mathematical model in terms of a third-order (jerk) nonlinear differential equation, or equivalently, a system of three first-order differential equations. The analysis shows that this system has three collinear equilibrium points. The time waveform and the trajectories about each equilibrium point depend on its associated eigenvalues. We prove that all three equilibrium points are of type saddle focus, meaning that the trajectory of $(x(t), y(t))$ diverges in a spiral form but $z(t)$ converges to the equilibrium point for any initial point $(x(0), y(0), z(0))$. Numerical simulation illustrates that the oscillations are dense, have no period, are highly sensitive to initial conditions, and have a chaotic hidden attractor.

Keywords: chaos theory, electrical circuit analysis, jerk circuit, Chua's diode, system of differential equations, hidden attractor.

PACS: 02.10.Ud; 02.30.Hq; 05.45.Pq; 84.32.-y

1. Introduction

Nowadays, chaos theory is an important subject dealing with physics, mathematics, and engineering. A chaos system is a nonlinear dynamical system that has a non-periodic oscillation of waveforms. It is sensitive to initial conditions and has the self-similarity property. A significant development of chaos theory is the discovery of the celebrated Chua's system by L.O. Chua in 1983. This system was described by a set of three first-order ordinary differential equations (ODEs). Chua's discovery has encouraged others to look for more chaotic systems, for example, systems of the type Rössler, jerk [1,2], circulant [3,4], hyperjerk [5,6], and hyperchaotic [5,7,8]. In addition, several chaotic circuits have been investigated, for example, Lorenz-based chaotic circuits [9,10], Chua's circuits [11–14], Wien-type chaotic oscillator [15], and chaotic jerk circuits [16–19]. Chaos theory has increasingly attracted much attention due to its wide applications in physical/natural/health sciences and engineering, for example, communication systems, weather forecasting, image encryption [20], celestial mechanics [21], population models [22], hydrology [23], cardiocography [24], and dynamical disease [25]. Chaos theory as formulated for physical dynamic systems turns out to be useful in social science. For example, chaos theory can be applied to a simple nonlinear model concerning arms race; see, for example [26,27]. The works [28,29] substantiate the chaotic phenomena in dynamic love affair models.

L.O. Chua [14] investigated the chaotic theory for a simple famous circuit in Figure 1, known nowadays as Chua's circuit. The circuit consists of only resistors, capacitors, and a nonlinear resistor. The nonlinear resistor, also called Chua's diode, consists of many op-amps. Many researchers

discussed several ways to modify the classical Chua's circuit to a more complicated circuit having chaotic phenomenon. Morgul [30] used an inductorless realization of a Chua's diode consisting of the Wien-bridge oscillator, coupled in parallel with the same nonlinear resistor used in the classical Chua's diode. Numerical experiments illustrated similar chaotic behavior. Aissi and Kazakos [31] modified the Chua's circuit by replacing the op-amps in Chua's diode with RC op-amps. Stouboulos et al. [32] modified the oscillator so that it consists of a nonlinear resistor and a negative conductance, demonstrating the birth and catastrophe of the double-bell strange attractor for different values of frequency. Kyprianidis [33] investigated the anti-monotonicity of the Chua's circuit, which is the creation of forward period-doubling bifurcation sequences followed by reverse period-doubling sequences. The work [34] of Kyprianidis and Fotiadou shows a possible way to replace the piecewise linear characteristic of the Chua's diode with a smooth cubic polynomial. Recently, the work [35] investigates chaotic behavior of the classical Chua's circuit with two nonlinear resistors. The existence of two nonlinear resistors in that case implies that the system has three equilibrium points.

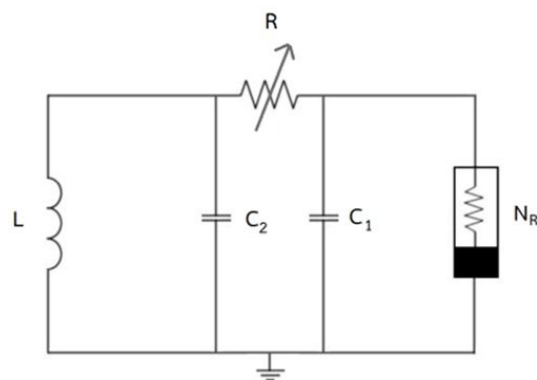


Figure 1. Chua's circuit [14].

In 2011, Sprott [19] studied a simple chaotic jerk circuit, as shown in Figure 2, consisting of only five electronic components: two capacitors, an inductor, an adaptive resistor and a nonlinear resistor. His work shows a chaotic behavior of the trajectories around the equilibriums of the system, and launches a quest for other circuits that chaotically oscillate. Indeed, this circuit can be formulated into a third-order ODE consisting of a nonlinear term, called a "jerk" or the third-order derivative of a variable.

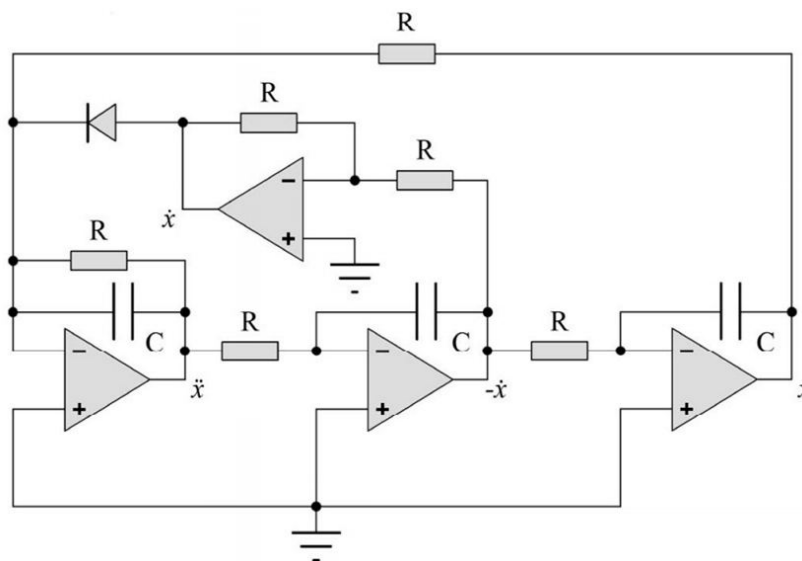


Figure 2. A chaotic jerk circuit [19].

According to much recent interest about chaotic oscillators based on jerk equations, this paper investigates the chaotic behavior of a new chaotic jerk circuit. We modify the chaotic jerk circuit in [19] so that there is a Chua's diode connected parallel to the nonlinear resistor as in Figure 3. The existence of Chua's diode discriminates the proposed system to the system [19]. The voltage-current characteristic of the Chua's diode satisfies a symmetric piecewise linear relation. To describe our system (see Section 2), we apply fundamental laws in electrical circuit theory to formulate a mathematical model in terms of a third-order (jerk) nonlinear ODE, or a system of three first-order ODE. The analysis in Section 3 shows that this system has three collinear symmetric equilibrium points. The time waveform about each equilibrium point depends on its associated eigenvalues. We prove that all three equilibrium points are of type saddle focus node, meaning that the trajectories of $(x(t), y(t))$ diverge in a spiral form but $z(t)$ converges to the equilibrium point for any initial value $(x(0), y(0), z(0))$. Numerical simulation in Section 4 illustrates the chaotic phenomenon, including time waveforms, trajectories about each equilibrium point, effects of changing initial points, and existence of a chaotic hidden attractor. Finally, we summarize the paper in Section 5. In particular, we compare our work to [14,19].

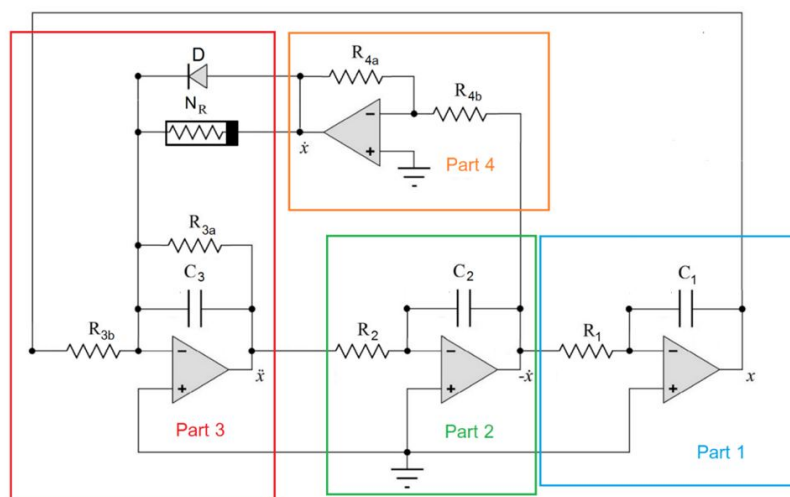


Figure 3. A modified chaotic jerk circuit with Chua's diode.

2. Formulation of a Modified Chaotic Jerk Circuit with Chua's Diode to a System of ODEs

In this section, we formulate a mathematical model for a modified chaotic jerk circuit with Chua's diode in terms of a system of ODEs concerning a piecewise linear function and exponential term. We divide the circuit into four parts, as illustrated in Figure 3. Our analysis is based on fundamental theory of electrical circuit analysis such as Ohm's law, Kirchhoff's current law (KCL) and Kirchhoff's voltage law (KVL).

For Part 1, using KCL and the current-voltage equation for the capacitor, we have

$$\frac{v_{R_1}}{R_1} = i_{R_1} = i_{C_1} = C_1 \frac{dv_{C_1}}{dt} = C_1 \dot{v}_{C_1}.$$

Now, since $v_{R_1} = v_{C_2}$, we obtain $\dot{v}_{C_1} = v_{C_2}/(R_1 C_1)$. Without loss of generality, we may normalize the value of $R_1 C_1$ to be 1 ms and we thus have

$$\dot{v}_{C_1} = v_{C_2}. \quad (1)$$

Similarly, for Part 2 we reach $\dot{v}_{C_2} = v_{C_3}/(R_2 C_2)$. Setting the time constant $R_2 C_2 := 1$ yields

$$\dot{v}_{C_2} = v_{C_3}. \quad (2)$$

For Part 3, we have by KCL that $i_{R_{3b}} + i_{N_R} + i_D = i_{R_{3a}} + i_{C_3}$. It follows that

$$\dot{v}_{C_3} = -\frac{v_{C_1}}{R_{3b}C_3} - \frac{v_{C_3}}{R_{3a}C_3} + \frac{i_{N_R}}{C_3} + \frac{i_D}{C_3}.$$

Setting the time constants $R_{3a}C_3$ and $R_{3b}C_3$ to be $1ms$, we get

$$\dot{v}_{C_3} = -v_{C_1} - v_{C_3} + R_{3a}(i_{N_R} + i_D). \quad (3)$$

The circuit in Figure 4 is a more complicated one since it consists of two nonlinear resistors. For the nonlinear resistor on the left, we have by Ohm's law that $v_{N_R} = i_{R_3}R_{3r}$, $v_e = (R_{2c} + R_{3c})i_{R_3}$ and $v_{N_R} - v_e = i_xR_1$, where v_e is the voltage of the op-amp on the left hand side. Combining these three equations to get $v_{N_R} = i_xR_x$ where

$$R_x = -\frac{R_{1c}R_{3c}}{R_{2c}}.$$

Similarly, for the nonlinear resistor on the right, we obtain that $v_{N_R} = i_yR_y$ where

$$R_y = -\frac{R_{4c}R_{6c}}{R_{5c}}.$$

Using KCL at node c , we have $i_{N_R} - i_x - i_y = 0$. Then the current i_{N_R} satisfies the relation

$$v_{N_R} = i_{N_R}(R_x + R_y).$$

However, as pointed out in [19], the behavior of i_{N_R} depends on the voltage v_{C_1} . Indeed, when $v_e < v_f$, the graph of i_{N_R} with respect to v_{C_1} is as follows:

From Figure 5, we have

$$i_{N_R} = \left(\frac{1}{R_x} + \frac{1}{R_{4c}}\right)v_{C_1} + \frac{1}{2}\left(\frac{1}{R_y} - \frac{1}{R_{4c}}\right)\left(\left|v_{C_1} + \frac{v_{f,max}}{v_f}v_{C_1}\right| - \left|v_{C_1} - \frac{v_{f,max}}{v_f}v_{C_1}\right|\right), \quad (4)$$

where $v_{f,max}$ is the maximum voltage at the node f . The current i_D through the diode D depends on the time-derivative of the voltage v_{C_1} (see, e.g., [18]) as follows:

$$i_D = k^2T^2e^{\dot{v}_{C_1}/kT},$$

where k is the Boltzmann constant and T is the absolute temperature of the P-N junction. Let us denote $\alpha := kT$. Of particular interest is that the chaos persists when α tends to zero. Since

$$\lim_{\alpha \rightarrow 0^+} \alpha^2 e^{y/\alpha} = \infty.$$

At Part 4, we use KCL to analyze this part and we get $i_{R_{4b}} = i_{R_{4a}}$. From Parts 2 and 4, we have by Ohm's law that $v_{C_2}/R_{4b} = v_{R_{4a}}/R_{4a}$ and, thus, the second capacitive voltage is

$$v_{C_2} = \frac{R_{4b}}{R_{4a}}v_{R_{4a}}.$$

For convenience, denote

$$m_0 = R_{3a}\left(\frac{1}{R_x} + \frac{1}{R_y}\right), \quad m_1 = R_{3a}\left(\frac{1}{R_x} + \frac{1}{R_{4c}}\right).$$

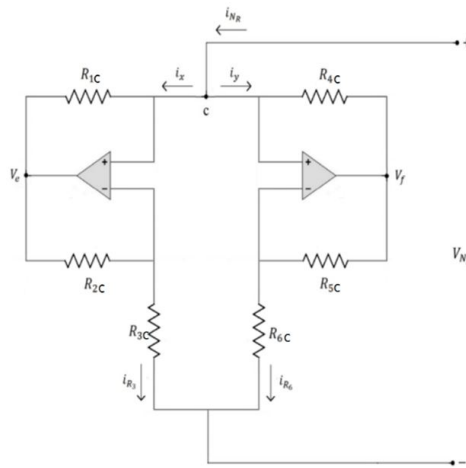


Figure 4. Two nonlinear resistors in Chua’s circuit.

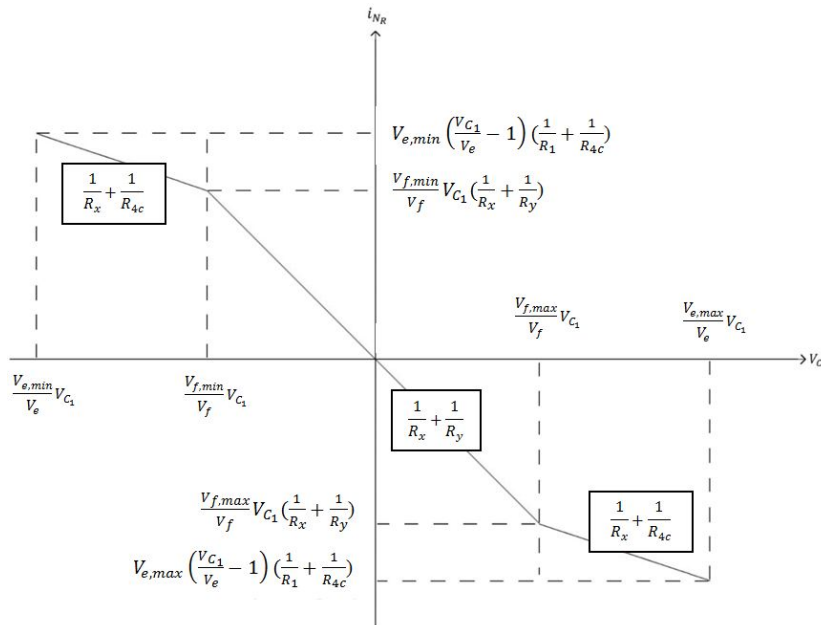


Figure 5. I-V characteristic of nonlinear resistors.

Let us rescale the variables v_{C1}, v_{C2}, v_{C3} to new variables x, y, z so that the current i_{NR} is reduced to

$$g(x) = m_1x + 0.5(m_0 - m_1) (|x + 1| - |x - 1|), \tag{5}$$

so that the characteristic in Figure 5 becomes that in Figure 6.

Thus, the third-order (jerk) system can be described by the group of Equations (1)–(3), or equivalently, the following system of three first-order ODEs:

$$\begin{aligned} \dot{x} &= y, \\ \dot{y} &= z, \\ \dot{z} &= -x - z + g(x) + \alpha^2 e^{\frac{y}{\alpha}}. \end{aligned} \tag{6}$$

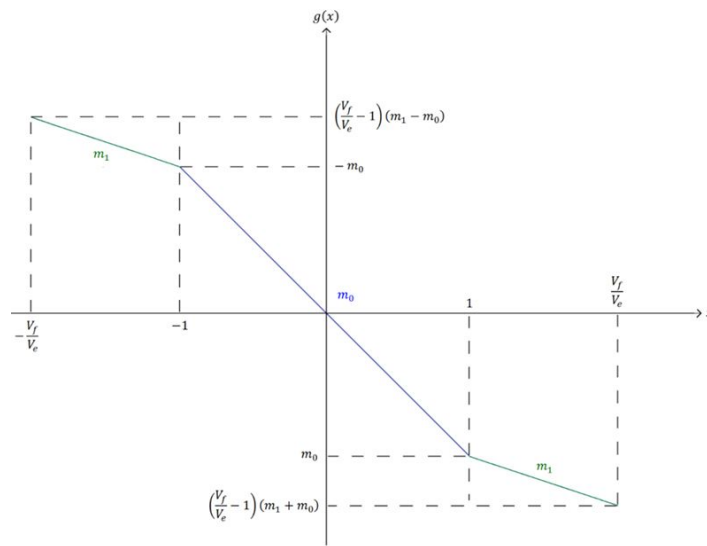


Figure 6. Changing scales of I-V characteristic of nonlinear resistors.

3. Analysis for Chaotic Behavior of the System

In order to analyze the behavior of the dynamical system (6), we need to find all its equilibrium points. Note that Figure 6 illustrates how the three-segment piecewise function $g(x)$ depends on the range of x . The investigation of equilibrium points is thus divided into three cases in Sections 3.1–3.3. We then prove that each equilibrium point is of type saddle focus in Section 3.4. In Section 3.5, we describe how to find an initial point to localize a hidden attractor of the system.

3.1. Case 1: $-1 < x < 1$

From Equation (5), we have $g(x) = m_0x$. At the equilibrium point, we get $y = \dot{x} = 0$, $z = \dot{y} = 0$, and

$$-x - z + m_0x + \alpha^2 e^{y/\alpha} = \dot{z} = 0.$$

Thus, the equilibrium for Case 1 is given by $E_1 = (x_1, y_1, z_1) = (\frac{\alpha^2}{1-m_0}, 0, 0)$. When α tends to 0, the equilibrium point reaches the origin $(0, 0, 0)$.

The system (6) can be put in the vector form

$$X'(t) = AX(t) + B(t), \tag{7}$$

where

$$X(t) = \begin{bmatrix} x(t) \\ y(t) \\ z(t) \end{bmatrix}, \quad B(t) = \begin{bmatrix} 0 \\ 0 \\ \alpha^2 e^{y(t)/\alpha} \end{bmatrix}, \quad A = \begin{bmatrix} 0 & 1 & 0 \\ 0 & 0 & 1 \\ m_0 - 1 & 0 & -1 \end{bmatrix}.$$

3.2. Case 2: $-\frac{v_f}{v_e} \leq x \leq -1$

In this case, we have $g(x) = m_1x - m_0 + m_1$. At the equilibrium point, we obtain $y = \dot{x} = 0$, $z = \dot{y} = 0$, and

$$-x - z + m_1x - m_0 + m_1 + \alpha^2 e^{y/\alpha} = \dot{z} = 0.$$

Thus, the equilibrium for Case 2 is given by

$$E_2 = (x_2, y_2, z_2) = \left(\frac{\alpha^2 - m_0 + m_1}{1 - m_1}, 0, 0 \right).$$

When $\alpha \rightarrow 0$, we have (x_2, y_2, z_2) reaches the point $\left(\frac{-m_0 + m_1}{1 - m_1}, 0, 0 \right)$. The system (6) can be put in the vector form (7) where

$$A = \begin{bmatrix} 0 & 1 & 0 \\ 0 & 0 & 1 \\ m_1 - 1 & 0 & -1 \end{bmatrix}, \quad B(t) = \begin{bmatrix} 0 \\ 0 \\ -m_0 + m_1 + \alpha^2 e^{y(t)/\alpha} \end{bmatrix}.$$

3.3. Case 3: $1 \leq x \leq \frac{v_f}{v_e}$

We have $g(x) = m_1 x + m_0 - m_1$ and, thus, the equilibrium point is given by

$$E_3 = (x_3, y_3, z_3) = \left(\frac{\alpha^2 + m_0 - m_1}{1 - m_1}, 0, 0 \right).$$

When $\alpha \rightarrow 0$, we have (x_3, y_3, z_3) reaches $\left(\frac{m_0 - m_1}{1 - m_1}, 0, 0 \right)$. We also have the vector form (7) where the Jacobian matrix A is the same as that in the previous case, and

$$B(t) = \begin{bmatrix} 0 \\ 0 \\ m_0 - m_1 + \alpha^2 e^{y(t)/\alpha} \end{bmatrix}.$$

Thus, the system (6) has three colinear equilibrium points on the X -axis. Note that when $\alpha \rightarrow 0$, we have that the points E_2 and E_3 are opposite to each other with respect to the origin E_1 . This observation shows the symmetry of the equilibrium points.

3.4. Type of Equilibrium Points

Recall the following theorem:

Theorem 1 (see, e.g., [36]). *Let $A(t) = [a_{ij}(t)] \in \mathbb{R}^{n \times n}$ be a continuous matrix-valued function on an interval I (i.e., each $a_{ij}(t)$ is a real-valued continuous function on I). Let $B(t) \in \mathbb{R}^n$ be a continuous vector-valued function on I . Then the following initial value problem*

$$X'(t) = A(t)X(t) + B(t), \quad X(0) = X_0,$$

has a unique solution $X(t) \in \mathbb{R}^n$ on the interval I .

This theorem guarantees the Equation (7) has a unique solution $X(t)$ on any time interval (note that, in this case, A is a constant matrix). Thus in all cases of x , given an initial point $(x(0), y(0), z(0))$, the trajectory of $(x(t), y(t), z(t))$ is uniquely determined. The trajectory of $(x(t), y(t), z(t))$ in a neighborhood of each equilibrium point depends on the signs of the real/imaginary parts of the eigenvalues of the coefficient matrix A .

For Case 1: $-1 < x < 1$, we have the characteristic equation

$$\det(\lambda I - A) = \lambda^3 + \lambda^2 + 1 - m_0 = 0.$$

Since all parameters of the equation are real and the equation degree is odd, we have that a root (says λ_1) is real and other roots are a conjugate pair of complex numbers. Note that $m_0 < 0$ from Figure 6. Now, the product of all roots (eigenvalues) satisfies

$$\lambda_1\lambda_2\lambda_3 = m_0 - 1 < 0.$$

Since (λ_2, λ_3) is a complex conjugate pair, the real root λ_1 must be negative. Write $\lambda_2 = a + ib$ and $\lambda_3 = a - ib$, where $a, b \in \mathbb{R}$. Since the sum of products of two roots of the cubic equation satisfies

$$\lambda_1\lambda_2 + \lambda_2\lambda_3 + \lambda_3\lambda_1 = 1,$$

we get

$$a^2 + 2\lambda_1 a + b^2 = 1.$$

Solving this quadratic equation to obtain

$$a = -\lambda_1 \pm \sqrt{\lambda_1^2 - b^2 - 1}.$$

Since $\lambda_1 < 0$ and $\sqrt{\lambda_1^2 - b^2 - 1} < |\lambda_1|$, we get $a > 0$. Hence, an eigenvalue is a negative real and two other eigenvalues are a conjugate pair of complex numbers having positive real parts. Therefore, this equilibrium is a saddle focus, and the trajectory of $(x(t), y(t))$ diverges in a spiral form, but $z(t)$ converges to the equilibrium point for any initial point $(x(0), y(0), z(0))$.

For Cases 2 and 3, the Jacobian matrices are the same and we have the characteristic equation

$$\det(\lambda I - A) = \lambda^3 + \lambda^2 + 1 - m_1 = 0.$$

Since $m_1 < 0$ (from Figure 6), we obtain the same conclusion as in Case 1, i.e., the equilibrium point is a saddle focus.

We summarize the above discussion in the following theorem:

Theorem 2. *The system (6) has three equilibrium points, each of which is of type saddle focus. Moreover, the trajectory of $(x(t), y(t))$ diverges in a spiral form, but $z(t)$ converges to the equilibrium point for any initial point $(x(0), y(0), z(0))$.*

Since the equilibrium points are saddle foci, our system has chaotic behavior.

3.5. Localization of a Hidden Attractor of The System

Recall that an oscillation in a dynamical system can be numerically localized if an initial condition from its neighborhood leads to asymptotic behavior. Such an oscillation is known as an attractor, and its attracting set is called the basin of attraction. If the basin of attraction intersects a small neighborhood of an equilibrium point, then such attractor is said to be self-excited; otherwise it is called a hidden attractor. The hidden attractor was discovered in [37] for a generalized Chua's circuit, and then was discovered in the classical Chua's circuit [38].

In order to find a hidden attractor of the system, we will find a suitable initial point $(x(0), y(0), z(0))$ so that our system will have chaos. First, let us write the system (6) into a first-order vector differential equation

$$X'(t) = AX(t) + \psi(r^T X(t))q \quad (8)$$

where $X(t) = [x(t) \ y(t) \ z(t)]^T \in \mathbb{R}^3$, $A \in \mathbb{R}^{3 \times 3}$, $r \in \mathbb{R}^3$, $q \in \mathbb{R}^3$, and $q : \mathbb{R} \rightarrow \mathbb{R}$ is a continuous piecewise-differentiable function. Here, $(\cdot)^T$ denotes the transposition operation. To find a periodic

oscillation, we introduce a coefficient k of harmonic linearization so that the matrix $A_0 = A + kqr^T$ of the linear system

$$X'(t) = A_0X(t)$$

has a pair of pure-imaginary eigenvalues $\pm i\omega_0$ for some $\omega_0 > 0$, and the rest of the eigenvalues have negative real parts. Then the system (8) has a periodic solution $X(t)$ such that

$$\sigma(t) := r^T X(t) \approx a \cos \omega_0 t,$$

where the amplitude a is a solution of the integral equation

$$\int_0^{2\pi/\omega_0} (\psi(a \cos \omega_0 t)) a \cos \omega_0 t - k(a \cos \omega_0 t)^2 dt = 0.$$

Denoting $\phi(\sigma) = \psi(\sigma) - k\sigma$, we can write Equation (8) to

$$X'(t) = A_0X(t) + q\phi(r^T x).$$

Let us change $\phi(\sigma)$ to $\epsilon\phi(\sigma)$ where ϵ is a small positive number, and investigate a periodic solution of the system

$$X'(t) = A_0X(t) + \epsilon q\phi(r^T x). \quad (9)$$

Let us introduce the describing function

$$\Phi(a) = \int_0^{2\pi/\omega_0} \phi(a \cos(\omega_0 t)) \cos(\omega_0 t) dt.$$

We make an invertible linear transformation $X(t) = SY(t)$ where $S \in \mathbb{R}^{3 \times 3}$ is a nonsingular matrix. The following theorem tells us how to choose an initial point in order to get a hidden attractor of the system.

Theorem 3 ([39]). *If there is a positive number a_0 such that $\Phi(a_0) = 0$ and $b_1\Phi'(a_0) < 0$, then the system (9) has a stable periodic solution with initial point*

$$X(0) = S[y_1(0) \ y_2(0) \ y_3(0)]^T$$

where $y_1(0) = a_0 + O(\epsilon)$, $y_2(0) = 0$, and $y_3 = O_{n-2}(\epsilon)$ with period $O(\epsilon) + \frac{2\pi}{\omega_0}$.

4. Numerical Experiment

In this section, we provide a numerical experiment to illustrate the chaotic behavior of the proposed circuit via MATLAB. Consider the circuit in Figure 3 with the following parameters: $R_1 = 1 \text{ k}\Omega$, $R_2 = 200 \ \Omega$, $R_{3a} = 500 \ \Omega$, $R_{3b} = 500 \ \Omega$, $R_{4a} = 1 \text{ k}\Omega$, $R_{4b} = 1 \text{ k}\Omega$, $R_{1c} = 250 \ \Omega$, $R_{2c} = 250 \ \Omega$, $R_{3c} = 500 \ \Omega$, $R_{4c} = 750 \ \Omega$, $R_{5c} = 180 \ \Omega$, $R_{6c} = 400 \ \Omega$, $C_1 = 1 \ \mu\text{F}$, $C_2 = 5 \ \mu\text{F}$, $C_3 = 2 \ \mu\text{F}$, $m_0 = -0.1768$, $m_1 = -1.1468$, and $\alpha = 0.026077$. We set the initial condition to be $X(0) = (x(0), y(0), z(0)) = (0, -0.7, 0)$.

Remark 1. *In order to obtain the chaotic phenomenon, one can adjust some parameter values of electronics devices in the circuit so that the eigenvalues of the Jacobian matrix satisfy the condition for the type of equilibrium point (see Section 3.4).*

4.1. Mathematical Analysis of the System

For the case of $-1 < x < 1$, the equilibrium points of the system are given by

$$E_1 = \left(\frac{\alpha^2}{1 - m_0}, 0, 0 \right) = (5.77838 \times 10^{-4}, 0, 0).$$

In this case, we reach the system $X'(t) = AX(t) + B(t)$ where

$$A = \begin{bmatrix} 0 & 1 & 0 \\ 0 & 0 & 1 \\ -1.1768 & 0 & -1 \end{bmatrix}, \quad B(t) = \begin{bmatrix} 0 \\ 0 \\ \alpha^2 e^{y(t)/\alpha} \end{bmatrix}.$$

The eigenvalues of the system associated with the equilibrium point E_1 are the solutions of the cubic equation

$$\lambda^3 + \lambda^2 + 1.1768 = 0.$$

We get the following eigenvalues

$$\lambda_1 = -1.51364, \quad \lambda_2 = 0.25682 + 0.84351i, \quad \lambda_3 = 0.25682 - 0.84351i.$$

For the case $-v_f/v_e \leq x \leq -1$, we can obtain the equilibrium point

$$E_2 = \left(\frac{\alpha^2 - m_0 + m_1}{1 - m_1}, 0, 0 \right) = (-0.969422, 0, 0)$$

associated with eigenvalues

$$\lambda_1 = -1.72307, \quad \lambda_2 = 0.36154 + 1.05603i, \quad \lambda_3 = 0.36154 - 1.05603i.$$

For the case $1 \leq x \leq v_f/v_e$, the system has the equilibrium point $E_3 = (0.452152, 0, 0)$. Note that E_2 and E_3 have the same eigenvalues since their associated matrices are the same.

From the signs of real/imaginary parts of the associated eigenvalues, we conclude that the three equilibrium points E_1, E_2, E_3 are saddle foci. Hence, the proposed circuit has a chaotic behavior.

4.2. Time Waveforms and Trajectories of The System

The time waveforms of $x(t)$, $y(t)$ and $z(t)$ are reported in Figures 7–9, where the time interval is in *ms*. We see that the oscillations in the figures are non-periodic.

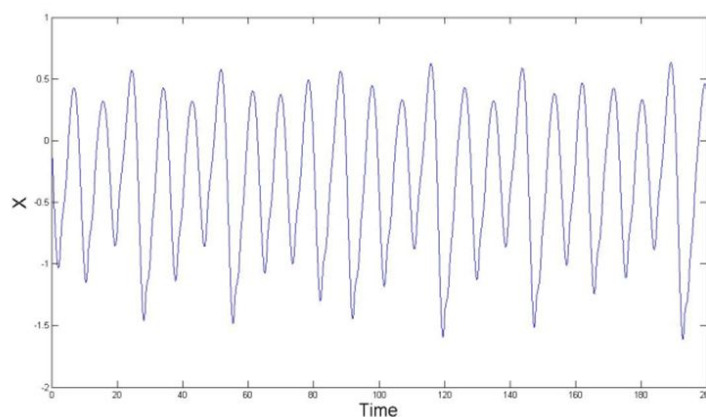


Figure 7. The time waveform of $x(t)$.

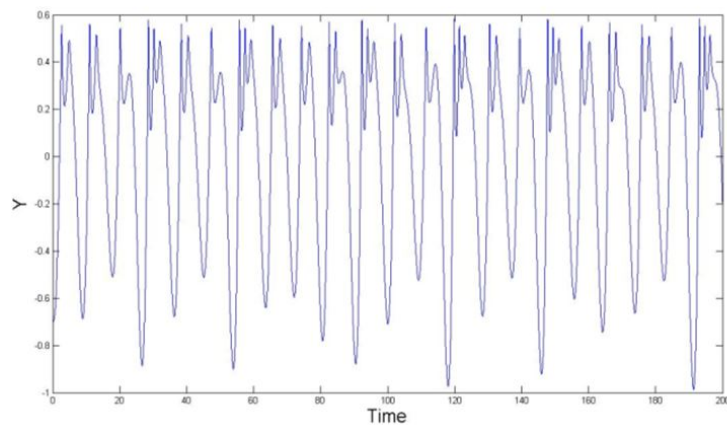


Figure 8. The time waveform of $y(t)$.

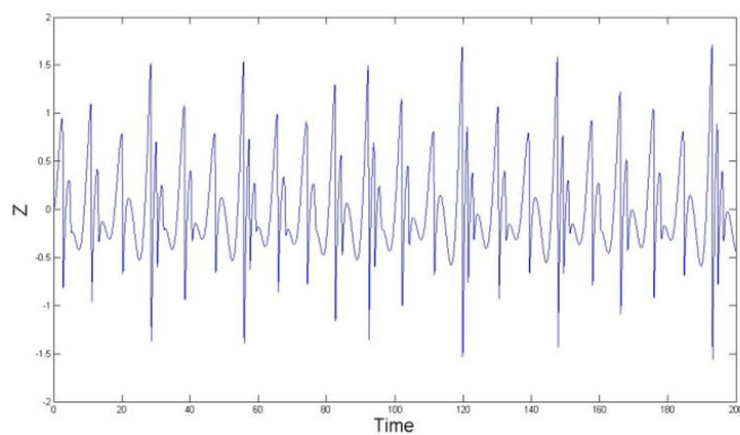


Figure 9. The time waveform of $z(t)$.

The trajectories of $x(t), y(t), z(t)$ in 2D and 3D are numerically simulated in Figures 10–13. We see that the trajectory of $(x(t), y(t))$ diverges in a spiral form, but $z(t)$ converges to the equilibrium point. The trajectories are dense and seem to have no periodic. Thus, chaotic behavior occurs in the modified jerk circuit with Chua's diode. Moreover, the attractor of the system is shown by the blue lines in Figures 10–13. From the 3D plot in Figure 13, we see that the oscillation does not connect with the equilibrium points E_1, E_2, E_3 , thus the system has a hidden attractor.

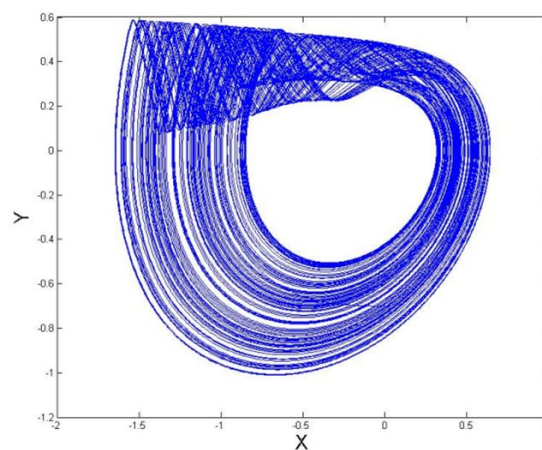


Figure 10. The trajectories of $(x(t), y(t))$ in 2D.

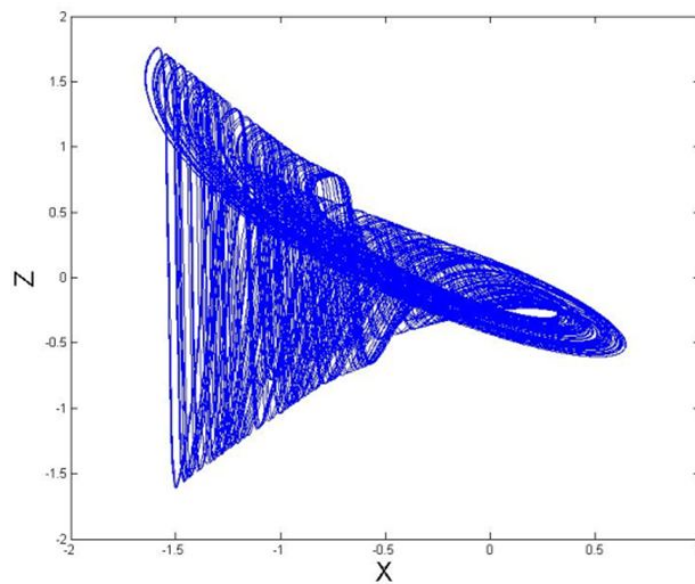


Figure 11. The trajectories of $(x(t), z(t))$ in 2D.

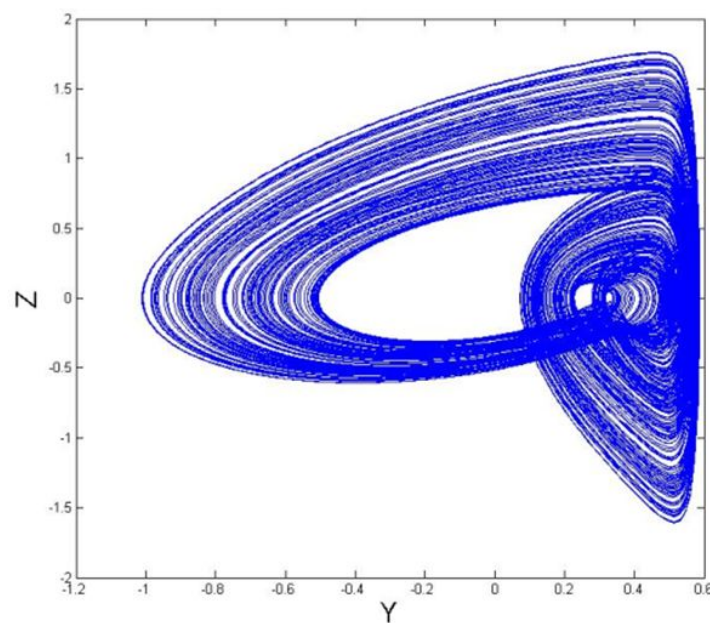


Figure 12. The trajectories of $(y(t), z(t))$ in 2D.

4.3. Effects of Changing Initial Points

Now, we investigate the effect of changing initial points. First, we compare the system behavior when initial values have small changes in the X-axis, namely, $I_1 = (0, -0.7, 0)$ and $I_2 = (0.0001, -0.7, 0)$; see Figure 14. Next, we consider the case of small changes in the Y-axis, namely, $I_1 = (0, -0.7, 0)$ and $I_2 = (0, -0.7001, 0)$; the resulting simulation is shown in Figure 15. Finally, the effect of small changes in the Z-axis of the initial point, namely, $I_1 = (0, -0.7, 0)$ and $I_2 = (0, -0.7, 0.0001)$ is illustrated in Figure 16.

From Figures 14–16, we see that a small difference in initial points leads to a big difference in oscillations of $x(t)$, $y(t)$, $z(t)$. Thus our dynamical system is highly sensitive to initial conditions, a characteristic of a chaotic system.

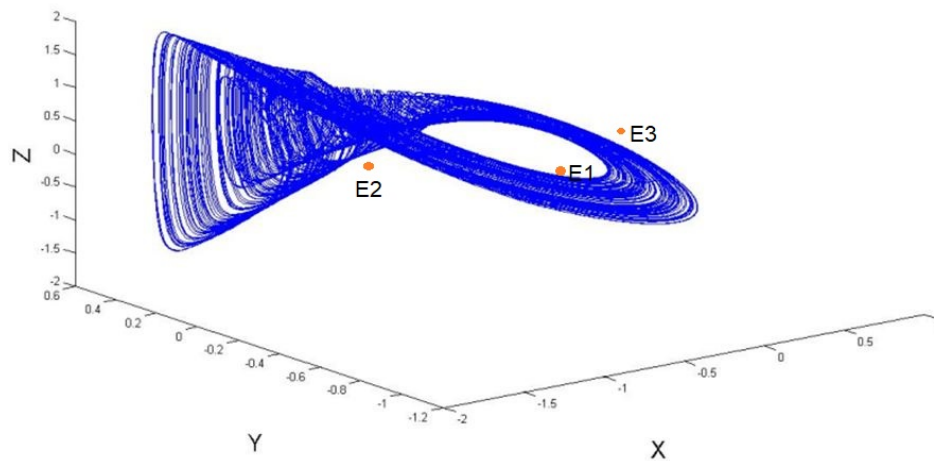


Figure 13. The trajectories of $(x(t), y(t), z(t))$ in 3D.

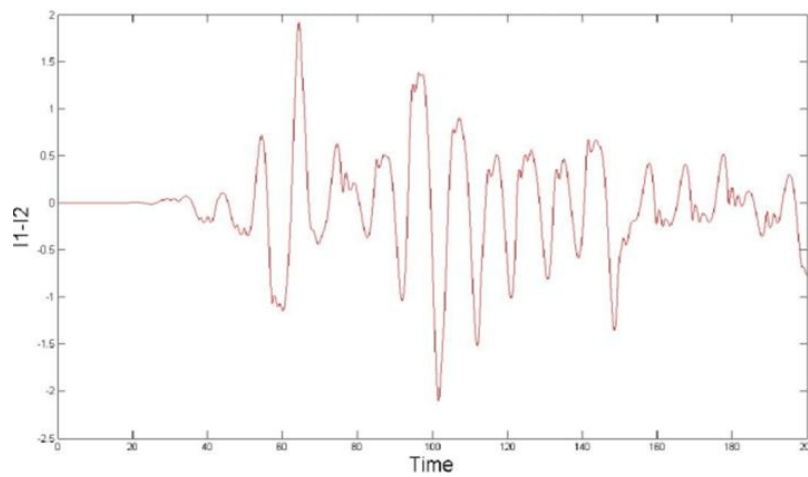


Figure 14. Effects of changing initial points in X-axis from $I1 = (0, -0.7, 0)$ to $I2 = (0.0001, -0.7, 0)$.

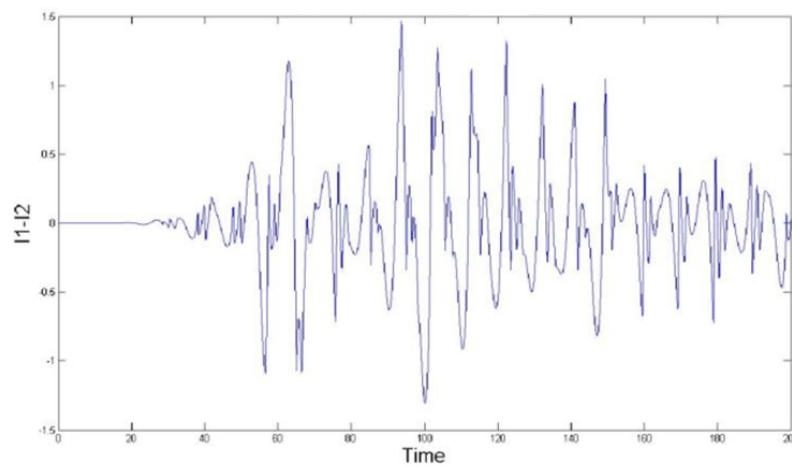


Figure 15. Effects of changing initial points in Y-axis from $I1 = (0, -0.7, 0)$ to $I2 = (0, -0.7001, 0)$.

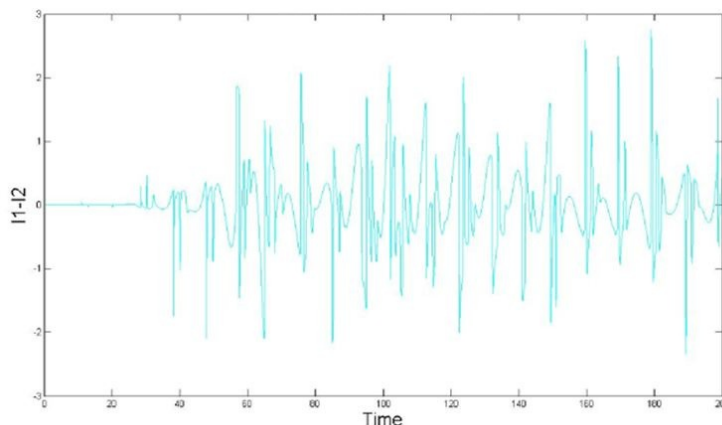


Figure 16. Effects of changing initial points in Z-axis from $I1 = (0, -0.7, 0)$ to $I2 = (0, -0.7, 0.0001)$.

5. Conclusions

We modify a jerk circuit with Chua’s diode, and investigate its chaotic properties. This system can be mathematically described by a system of ordinary differential equations with a piecewise linear function and exponential term. The analysis shows that this system has three collinear equilibrium points. The time waveform about each equilibrium point depends on its associated eigenvalues. Indeed, all three equilibrium points are of type saddle focus, meaning that the trajectories of $x(t)$ and $y(t)$ diverge in a spiral form but $z(t)$ converges to the equilibrium point for any initial point $(x(0), y(0), z(0))$. Numerical simulation illustrates that the oscillations are dense, have no period, are highly sensitive to initial conditions, and has a chaotic hidden attractor. Table 1 shows the comparison between three chaotic systems: the proposed system in this paper and the two existing systems in [14,19]. One of the advantages of the proposed system is a higher sensitivity to initial conditions. Therefore, the proposed system enables an alternative model for chaotic theory.

Table 1. The comparisons of a modified chaotic jerk circuit and other related systems.

No.	Terms of Comparison	Ref. [19]	Ref. [14]	This Paper
1	Number of equilibrium points	1	3	3
2	Number of eigenvalues	3	9	9
3	Types of trajectories	1 saddle focus node	1 stable focus node and 2 saddle foci	3 saddle foci
4	Number of components	14	5	15
5	Positions of equilibrium points	a point	3 symmetric points	3 symmetric points
6	Jerk-circuit type	yes	no	yes
7	Existence of Chua’s diode	no	yes	yes
8	Existence of chaotic attractors	yes	yes	yes
9	Sensitivity to initial conditions	$\sqrt{\sqrt{\sqrt{}}}$	$\sqrt{}$	$\sqrt{\sqrt{\sqrt{}}}$
10	Nonlinear system	yes	yes	yes

Funding: The author would like to thank King Mongkut’s Institute of Technology Ladkrabang Research Fund, grant no. KREF046205 for financial supports.

Acknowledgments: This work was supported by King Mongkut’s Institute of Technology Ladkrabang.

Conflicts of Interest: The author declares no conflict of interest.

References

1. Sprott, J.C. Some simple chaotic jerk functions. *Am. J. Phys.* **1997**, *65*, 537–543. [[CrossRef](#)]
2. Sprott, J.C. *Elegant Chaos: Algebraically Simple Chaotic Flows*; World Scientific: Singapore, 2010.
3. Lorenz, E.N.; Emanuel, K.A. Optimal sites for supplementary weather observations: Simulation with a small model. *J. Atmos. Sci.* **1998**, *55*, 399–414. [[CrossRef](#)]
4. Thomas, R. Deterministic chaos seen in terms of feedback circuits: Analysis, synthesis, ‘labyrinth chaos. *Int. J. Bifurcat. Chaos Appl. Sci. Eng.* **1999**, *9*, 1889–1905. [[CrossRef](#)]
5. Chlouverakis, K.E.; Sprott, J.C. Chaotic hyperjerk systems. *Chaos Solit. Frac.* **2006**, *28*, 739–746. [[CrossRef](#)]
6. Mumuangsaen, B.; Srisuchinwong, B. Elementary chaotic snap flows. *Chaos Solit. Frac.* **2011**, *44*, 995–1003. [[CrossRef](#)]
7. Rössler, O.E. An equation for hyperchaos. *Phys. Lett. A* **1979**, *71*, 155–157. [[CrossRef](#)]
8. Liu, Z.; Lai, Y.C.; Matias, M.A. Universal scaling of Lyapunov exponents in coupled chaotic oscillators. *Phys. Rev. E* **2003**, *67*, 1–4. [[CrossRef](#)] [[PubMed](#)]
9. Cuomo, K.M.; Oppenheim, A.V. Circuit implementation of synchronized chaos with applications to communications. *Phys. Rev. Lett.* **1993**, *71*, 65–68. [[CrossRef](#)]
10. Blakely, J.N.; Eskridge, M.B.; Corron, N.J. A simple Lorenz circuit and its radio frequency implementation. *Chaos* **2007**, *17*, 1–5. [[CrossRef](#)]
11. Matsumoto, T.; Chua, L.O.; Komuro, M. The double scroll. *IEEE Trans. Circuits Syst.* **1985**, *32*, 797–818. [[CrossRef](#)]
12. Bartissol, P.; Chua, L.O. The double hook. *IEEE Trans. Circuits Syst.* **1988**, *35*, 1512–1522. [[CrossRef](#)]
13. Chua, L.O.; Lin, G.-N. Canonical realization of Chua’s circuit family. *IEEE Trans. Circuits Syst.* **1990**, *37*, 885–902. [[CrossRef](#)]
14. Chua, L.O. The genesis of Chua’s circuit. *Archiv. Elektron. Übertragungstechnik* **1992**, *46*, 250–257.
15. Elwakil, A.S.; Kennedy, M.P. High frequency Wien-type chaotic oscillator. *Electron Lett.* **1998**, *34*, 1161–1162. [[CrossRef](#)]
16. Srisuchinwong, B.; Treetanakorn, R. Current-tunable chaotic jerk circuit based on only one unity-gain amplifier. *Electron Lett.* **2014**, *50*, 1815–1817. [[CrossRef](#)]
17. Srisuchinwong, B.; Nopchinda, D. Current-tunable chaotic jerk oscillator. *Electron Lett.* **2013**, *49*, 587–589. [[CrossRef](#)]
18. Sprott, J.C. Simple chaotic systems and circuits. *Am. J. Phys.* **2000**, *68*, 758–763. [[CrossRef](#)]
19. Sprott, J.C. A new chaotic jerk circuit. *IEEE Trans. Circuits Syst. II* **2011**, *58*, 240–243. [[CrossRef](#)]
20. Xu, M. Cryptanalysis of an image encryption algorithm based on DNA sequence operation and hyper-chaotic system. *3D Res.* **2017**, *8*, 15–24. [[CrossRef](#)]
21. Morbidelli, A. Chaotic diffusion in celestial mechanics. *Regul. Chaotic Dyn.* **2001**, *6*, 339–353. [[CrossRef](#)]
22. Eduardo, L.; Ruiz, A. Chaos in discrete structured population models. *SIAM J. Appl. Dyn. Syst.* **2012**, *11*, 1200–1214.
23. Sivakumar, B. Chaos theory in hydrology: Important issues and interpretations. *J. Hydrol.* **2000**, *227*, 1–20. [[CrossRef](#)]
24. Bozóki, Z. Chaos theory and power spectrum analysis in computerized cardiocography. *Eur. J. Obstet. Gynecol. Reprod. Biol.* **1997**, *71*, 163–168. [[CrossRef](#)]
25. Glass, L. Dynamical Disease: The Impact of Nonlinear Dynamics and Chaos on Cardiology and Medicine. In *The Impact of Chaos on Science and Society*; Grebogi, C., Yorke, J.A., Eds.; United Nations University Press: Tokyo, Japan, 1997.
26. Saperstain, A.M. Chaos—a model for the outbreak of war. *Nature* **1984**, *309*, 303–305. [[CrossRef](#)]
27. Grossmann, S.; Mayer-Kress, G. Chaos in the international arms race. *Nature* **1989**, *337*, 702–704. [[CrossRef](#)]
28. Huang, L.; Bae, Y. Analysis of chaotic behavior in a novel extended love model considering positive and negative external environment. *Entropy* **2018**, *20*, 365, doi:10.3390/e20050365 [[CrossRef](#)]
29. Yoon, J.H.; Bak, G.M. Youngchul Bae, Fuzzy control for chaotic confliction model. *Int. J. Fuzzy Syst.* **2020**, *22*, 1961–1971. [[CrossRef](#)]
30. Morgul, O. Inductorless realization of Chua oscillator. *Electron. Lett.* **1995**, *31*, 1403–1404. [[CrossRef](#)]

31. Aissi, C.; Kazakos, D. An improved realization of the Chua's circuit using RC-op amps. In Proceedings of the WSEAS International Conference on Signal Processing, Istanbul, Turkey, May 27-30, 2008; Volume 7, pp. 115–118.
32. Stouboulos, I.N.; Kyprianidis, I.M.; Papadopoulou, M.S. Complex chaotic dynamics of the double-bell attractor. *WSEAS Trans. Circuits Syst.* **2008**, *7*, 13–21.
33. Kyprianidis, I.M. New chaotic dynamics in Chua's canonical circuit. *WSEAS Trans. Circuits Syst.* **2006**, *5*, 1626–1633.
34. Kyprianidis, I.M.; Fotiadou, M.E. Complex dynamics in Chua's canonical circuit with a cubic nonlinearity. *WSEAS Trans. Circuits Syst.* **2006**, *5*, 1036–1043.
35. Lymphodaen, L.; Chansangiam, P. Mathematical analysis for classical Chua's circuit with two nonlinear resistors. *Songklanakarin J. Sci. Technol.* **2020**, *42*, 678–687.
36. Goode, S.W. *Differential Equations and Linear Algebra*; Prentice Hall: Englewood Cliffs, NJ, USA, 2000.
37. Kuznetsov, N.V.; Leonov, G.A.; Vagitsev, V.I. Analytical-numerical method for attractor localization of generalized Chua's system. *Int. Fed. Autom. Control. Proc.* **2010**, *4*, 29–33. [[CrossRef](#)]
38. Leonov, G.A.; Kuznetsov, N.V.; Vagitsev, V. Localization of hidden Chua's attractors. *Phys. Lett. A* **2011**, *375*, 2230–2233. [[CrossRef](#)]
39. Leonov, G.A.; Kuznetsov, N.V. Hidden attractors in dynamical systems. From hidden oscillations in Hilbert-Kolmogorov, Aizerman, and Kalman problems to hidden chaotic attractors in Chua circuits. *Int. Bifurc. Chaos* **2013**, *23*. [[CrossRef](#)]

Publisher's Note: MDPI stays neutral with regard to jurisdictional claims in published maps and institutional affiliations.



© 2020 by the author. Licensee MDPI, Basel, Switzerland. This article is an open access article distributed under the terms and conditions of the Creative Commons Attribution (CC BY) license (<http://creativecommons.org/licenses/by/4.0/>).